Designing Nanoporous Membranes through Templateless Electropolymerization of Thieno[3,4-b]thiophene Derivatives with High Water Content

El Hadji Yade Thiam, Abdoulaye Dramé, Salif Sow, Aboubacary Sene, Caroline R Szczepanski, Samba Yandé Dieng, Frédéric Guittard, Thierry Darmanin

Designing Nanoporous Membranes through Templateless Electropolymerization of Thieno[3,4-b]thiophene Derivatives with High Water Content

El hadji Yade Thiam,[†] Abdoulaye Dramé,[†] Salif Sow,[†] Aboubacary Sene,[†] Caroline R. Szczepanski,[§] Samba Yandé Dieng,[†] Frédéric Guittard,[‡,∥] and Thierry Darmanin*,[‡]

[†]Faculté des Sciences et Techniques, Département de Chimie, Université Cheikh Anta Diop, B.P. 5005 Dakar, Senegal

[‡]NICE Lab, IMREDD, Université Côte d'Azur, 61−63 Avenue Simon Veil, 06200 Nice, France

[§]Department of Chemical and Biological Engineering, Northwestern University, Evanston, Illinois 60208, United States

[∥]Department of Bioengineering, University California Riverside, Riverside, California 92521, United States

S Supporting Information

ABSTRACT: In this work, we present the synthesis of original thieno[3,4-b]thiophene monomers with rigid substituents (e.g., perfluorinated chains, and aromatic groups) and demonstrate the ability to prepare nanotubular and nanoporous structures via templateless, surfactant-free electropolymerization in organic solvents (dichloromethane). For the majority of synthesized monomers, including a significant amount of water in the electropolymerization solvent leads to the formation of nanoporous membranes with tunable size and surface hydrophobicity. If water is not included in the electropolymerization solvent, most of the surfaces prepared are relatively smooth. Tests with different water contents show that the formation of nanoporous membranes pass through the formation of vertically aligned nanotubes and that the increase in water content induces an increase in the number of nanotubes while their diameter and height remain unchanged. An increase in surface hydrophobicity is observed with the formation of nanopores up to ≈300 nm in diameter, but as the nanopores further increase in diameter, the surfaces become more hydrophilic with an observed decrease in the water contact angle. These materials and the ease with which they can be fabricated are extremely interesting for applications in separation membranes, opto-electronic devices, as well as for sensors.
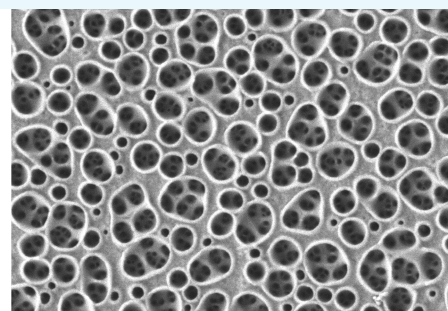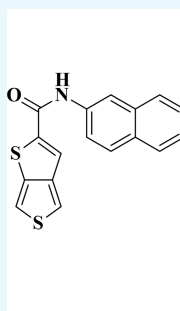
1. INTRODUCTION

Because of their large surface area, nanoporous interfaces such as nanotube arrays have gathered significant interest over recent years. Applications of interest for these interfaces include optical and electronic devices, sensors, as well as for the manipulation of surface wetting properties.[1−8] Similar to what has been observed and studied on natural surfaces with nanotubular arrays (e.g., Gecko pads), both surface hydrophobicity and water adhesion of nanoporous interfaces are highly dependent on the geometry of nanotube arrays (e.g., diameter, height, pore size, and spacing between nanotube features).[3−8] In order to develop these well-ordered surfaces, researchers often rely on hard or rigid templates such as anodized aluminum/titanium membranes to direct the formation of tubular and porous features.[9−13] Unfortunately, templated processes are lengthy and challenging to implement, especially on a large scale. Furthermore, a new template is needed for every desired modification to the surface geometry (e.g., changing diameter or spacing within the array).

To avoid the need for templates, researchers have recently become interested in using templateless electropolymerization as an alternative and rapid approach for the preparation of highly ordered, nanotube structures.[14] As one example, electropolymerization of pyrrole in aqueous solutions has been studied by many different research groups.[15−25] With pyrrole as the monomer, the in situ formation of porous structures is attributed to the release of gas bubbles (H_2 and/or O_2) from H_2O directly during electropolymerization. While the exploitation of this gas release is a relatively straightforward process, a surfactant is needed to stabilize the gas bubbles so the porous structures can readily form. More recent studies have identified approaches that eliminate the need for surfactants and thus permit the formation of tubular features via electropolymerization in organic solvents (e.g., CH_2Cl_2). In these studies, tubular features form only if trace H_2O is present

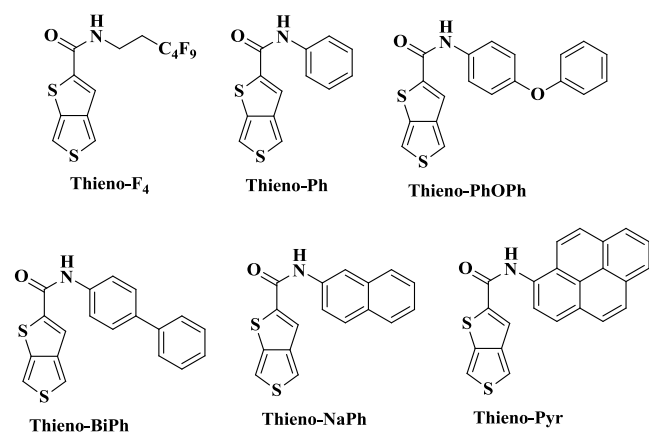in solution. Using this type of approach, vertically aligned nanotubes with high water adhesion have been developed using rigid monomers such as 3,4-phenylenedioxythiophene, naphthalenedioxythiophene, and thienothiophene derivatives.[26−31]

As demonstrated by prior research, thieno[3,4-b]thiophene monomers and associated analogues are excellent candidates to obtain nanotubular structures as well as hollow spheres via electrodeposition.[29−31] In this work, we demonstrate that with the judicious design of the thieno[3,4-b]thiophene monomer structure, it is possible to obtain nanoporous membranes with the tunable size and surface hydrophobicity. Rigid substituents (e.g., perfluorinated chains, aromatic groups) were incorporated into thieno[3,4-b]thiophene monomers (Scheme 1) and

their efficacy at electropolymerization was explored. We also highlight how the inclusion of water in the electropolymerization solvent significantly impacts the formation of porous structures.

2. RESULTS AND DISCUSSION

2.1. Templateless Electropolymerization. Electropolymerizations were performed in CH_2Cl_2 or $CH_2Cl_2 + H_2O$ solutions containing 0.1 M of Bu_4NClO_4 and 0.01 M of the monomer of interest. Cyclic voltammetry was chosen as the electrodeposition method because it enables robust polymer growth at an interface and also because it has the advantage of enabling precise characterization of the electrochemical phenomena. This includes monomer oxidation and polymerization, polymer oxidation and reduction, as well as water oxidation and reduction which has been shown to be responsible for producing O_2/H_2 gas bubbles.[29] For the monomers synthesized in this study, the oxidation potentials (E^{ox}) were determined to be ≈1.54−1.70 V versus saturated calomel electrode (SCE), depending on the structure. Using this information, electrodepositions were performed from −1 V to E^{ox} at a scan rate of 20 mV s^{-1}. In order to observe the polymer growth, the number of scans was varied (1, 3, or 5 scans).

Representative cyclic voltammograms for select monomers (thieno-F$_4$, thieno-BiPh, and thieno-NaPh) are presented in Figure 1. From these voltammograms, it is evident that the intensity of the polymer oxidation/reduction peaks is highest for thieno-F$_4$, thieno-Ph (not displayed), and thieno-PhOPh (not displayed). This is likely due to steric hindrance being the lowest with these substituents (Scheme 1). As a result, the

Scheme 1. Monomers Investigated in This Work

Thieno-F$_4$ Thieno-Ph   Thieno-PhOPh

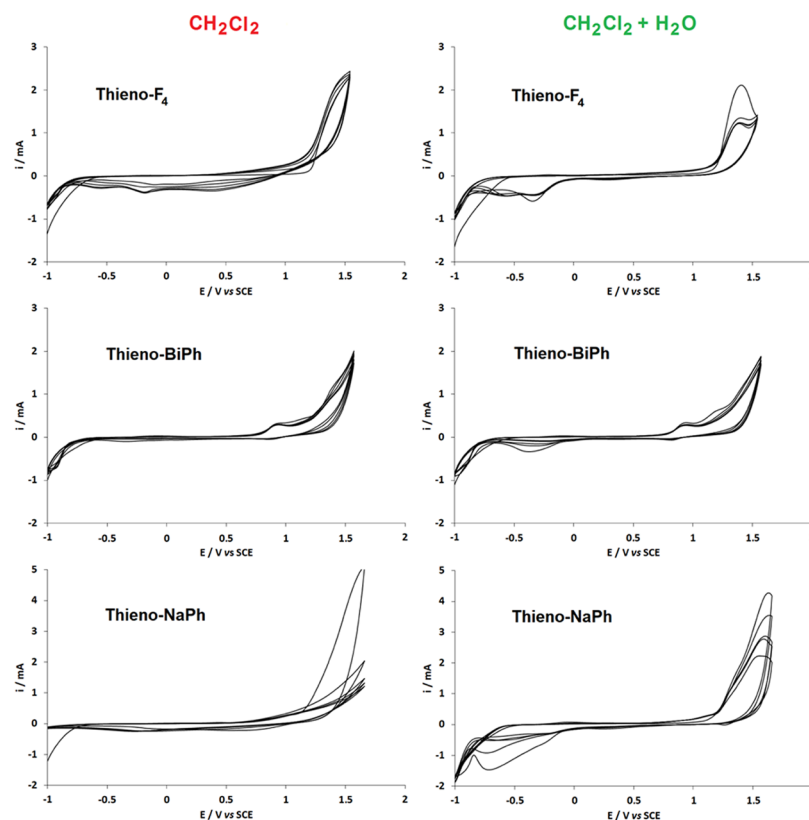Thieno-BiPh   Thieno-NaPh   Thieno-Pyr

CH_2Cl_2 $CH_2Cl_2 + H_2O$

Figure 1. Cyclic voltammograms (5 scans) of select monomers (thieno-F$_4$, thieno-BiPh, thieno-NaPh) in CH_2Cl_2 (left hand column) and CH_2Cl_2 + H_2O (right column) with Bu_4NClO_4 as the electrolyte. Scan rate: 20 mV s^{-1}.

thickness of the polymer deposited after cyclic voltammetry is greatest for these monomers. A small peak at ≈ -0.5 V versus SCE was also detected during the back scans with all the monomers, but this is particularly evident when the solvent is CH_2Cl_2 + H_2O. In prior works, this particular peak was found to be very important for the formation of porous structures and is attributed to the formation of H_2 bubbles from H_2O in solution $(2H_2O + 2e^- \rightarrow H_2$ (bubbles) $+ 2OH^-)$.[21,23] With the monomers studied here, this peak is particularly intense in the cyclic voltammogram of thieno-NaPh and thieno-Pyr. In the literature, it has been shown that the formation of O_2 bubbles from H_2O is possible during forward oxidation scans at roughly 1.5–2.0 V versus SCE $(2H_2O \rightarrow O_2$ (bubbles) $+ 4H^+ + 4e^-)$, which could also contribute to the development of porous structures. However, this process is more difficult to detect by cyclic voltammetry because the monomer oxidation occurs at roughly the same potentials $(n$monomer $\rightarrow$ polymer $+ 2ne^- + 2nH^+)$ and thus cannot be isolated in this study.

2.2. Surface Properties. The surface morphologies after electrodeposition via cyclic voltammetry (3 scans) of all monomers in both CH_2Cl_2 and CH_2Cl_2 + H_2O are highlighted in Figures 2 and 3. From these images, it is clear that including
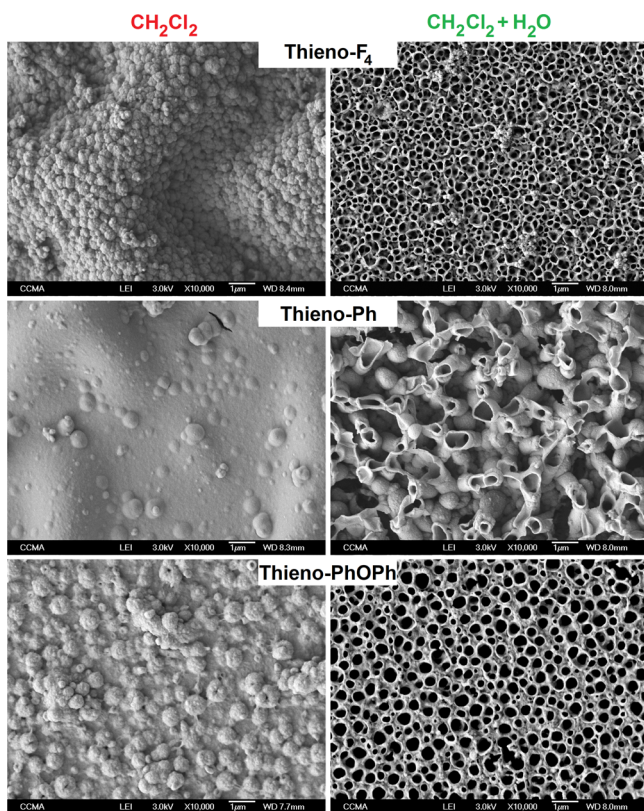

Figure 2. SEM images of polymer surfaces obtained from thieno-F$_4$, thieno-Ph, and thieno-PhOPh via cyclic voltammetry (3 scans) and using CH_2Cl_2 (left hand column) or CH_2Cl_2 + H_2O (right column) as the solvent.

water in the solvent mixture has a significant impact on the surface morphology. Most notably, all films prepared with CH_2Cl_2 as the solvent are nonporous (left-hand column, Figures 2 and 3). With thieno-Ph, thieno-BiPh, and thieno-NaPh, the surface morphology with CH_2Cl_2 as the solvent is ultimately very smooth. Wrinkles are observed for thieno-Pyr surfaces as well as more subtle wrinkles (that are less notable
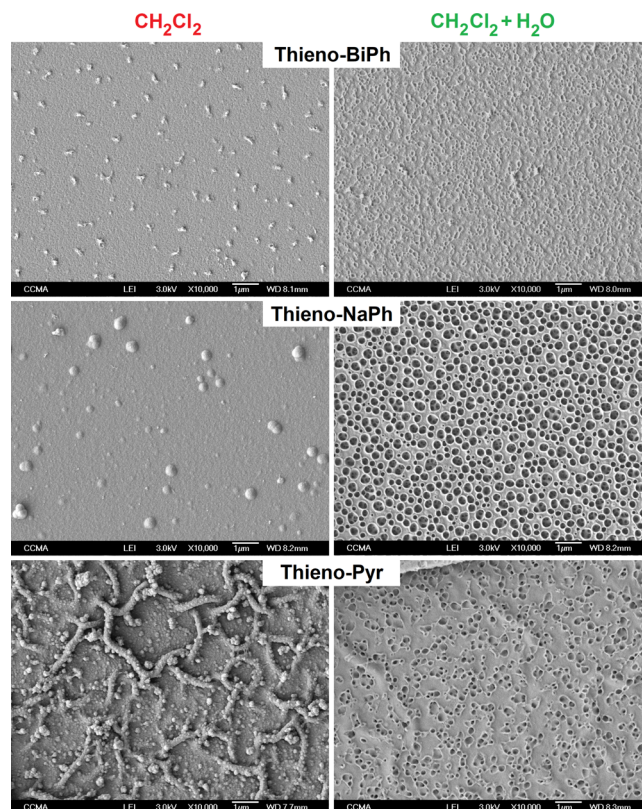

Figure 3. SEM images of polymer surfaces obtained from thieno-BiPh, thieno-NaPh, and thieno-Pyr via cyclic voltammetry (3 scans) and using CH_2Cl_2 (left hand column) or CH_2Cl_2 + H_2O (right column) as the solvent.

due to additional rough features) on thieno-F$_4$ films. Of all electropolymerizations conducted in CH_2Cl_2 as the solvent, the roughest surfaces form from thieno-F$_4$ and thieno-PhOPh (Figure 2). In these cases, the morphology consists of a high density of spherical particles across the surface, but as noted, the morphology is nonporous.

In contrast to the surfaces polymerized with CH_2Cl_2 as the solvent, the films prepared in CH_2Cl_2 + H_2O (right-hand columns, Figures 2 and 3) are porous. With thieno-Ph as the monomer, the morphology consists of tubular features, while nanoporous membranes are obtained with all other monomers. The pore size of the membranes is smallest with thieno-BiPh $(\emptyset \approx 100$ nm, Figure 3) and largest with thieno-PhOPh $(\emptyset \approx 500$ nm, Figure 2). Highly packed nanopores with homogenous distribution of the pore size $(\emptyset \approx 300$ nm) are observed in the case of thieno-Naph. As highlighted in Figure 4, for thieno-NaPh, the size of the pores does not vary with the number of deposition scans.

Surface hydrophobicity of all surfaces after electrodeposition was characterized via water contact angle measurements (Tables 1 and 2). The data reveal that thieno-F$_4$ surfaces have the strongest hydrophobic behavior, with $120° < \theta_w < 135°$ regardless of the solvent employed and the number of deposition scans (Tables 1 and 2). This result is expected, as the perfluorinated chains on the monomer structure significantly reduce overall surface energy. Furthermore, as demonstrated in Figure 2, rough surfaces result from electrodeposition of thieno-F$_4$ in CH_2Cl_2 and CH_2Cl_2 + H_2O, which following either the Cassie–Baxter or Wenzel

CH₂Cl₂ + H₂O
Thieno-NaPh
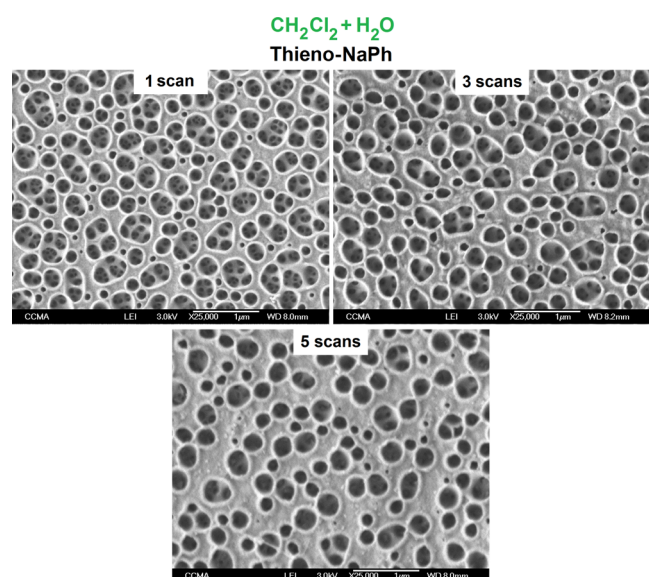

Figure 4. SEM images of polymer surfaces obtained from electro-deposition of thieno-NaPh in CH₂Cl₂ + H₂O via cyclic voltammetry after 1 (top, left), 3 (top, right), or 5 (bottom) scans.

Table 1. Wettability Data for the Polymer Films Obtained by Cyclic Voltammetry in CH₂Cl₂

polymer	number of deposition scans	θ_w [deg]
polythieno-F₄	1	120.2 ± 0.9
	3	134.5 ± 2.0
	5	130.9 ± 1.0
polythieno-Ph	1	78.6 ± 1.9
	3	94.4 ± 4.3
	5	103.7 ± 10.4
polythieno-PhOPh	1	72.1 ± 1.5
	3	86.0 ± 5.9
	5	108.1 ± 2.7
polythieno-BiPh	1	88.5 ± 10.5
	3	83.5 ± 2.6
	5	78.0 ± 4.1
polythieno-NaPh	1	81.8 ± 4.3
	3	84.8 ± 1.7
	5	85.4 ± 2.9
polythieno-Pyr	1	102.1 ± 2.7
	3	110.9 ± 7.5
	5	113.5 ± 5.9

wetting regimes of wetting will further enhance hydrophobic behavior.

Films obtained with thieno-BiPh and thieno-NaPh in CH₂Cl₂ are less hydrophobic with $\theta_w \approx 85°-88°$, regardless of the number of scans because of the relative smooth nature of these surfaces (Figure 3). Films obtained from thieno-Ph, thieno-PhOPh, and thieno-Pyr in CH₂Cl₂ have intermediate surface hydrophobicity; θ_w increases with the number of scans from 72° to 115°.

When the solvent is CH₂Cl₂ + H₂O, different wetting behavior is observed. With thieno-BiPh, $\theta_w \approx 80°$ and this value does not vary with the number of scans as the surfaces are relatively smooth (Figure 3). With thieno-NaPh as the monomer, the nanoporous structures have hydrophobic behavior as θ_w is as great as 112.4° (5 scans). Interestingly, despite having qualitatively similar porous features, the same is

Table 2. Wettability Data for the Polymer Films Obtained by Cyclic Voltammetry in CH₂Cl₂ + H₂O

polymer	number of deposition scans	θ_w [deg]
polythieno-F₄	1	123.5 ± 4.1
	3	131.7 ± 2.2
	5	124.3 ± 5.9
polythieno-Ph	1	83.7 ± 16.2
	3	86.6 ± 14.1
	5	120.1 ± 2.6
polythieno-PhOPh	1	84.4 ± 8.0
	3	65.9 ± 4.2
	5	73.5 ± 11.4
polythieno-BiPh	1	72.0 ± 5.9
	3	79.9 ± 3.7
	5	78.6 ± 1.0
polythieno-NaPh	1	107.3 ± 4.1
	3	89.0 ± 7.8
	5	112.4 ± 1.7
polythieno-Pyr	1	75.4 ± 3.5
	3	71.0 ± 4.5
	5	93.7 ± 4.1

not observed for thieno-PhOPh where hydrophobicity decreases slightly with the number of scans. Cases of increasing θ_w with increasing number of deposition scans (thieno-Ph, thieno-NaPh, thieno-Pyr) can be explained using the aforementioned Cassie−Baxter equation. This wetting regime assumes air is trapped inside nanoporous structures when a water droplet is deposited onto a surface, which causes increases in the observed θ_w.[32] Films with nanotubular structures (thieno-Ph) also displayed an increase θ_w up 120° with increasing number of deposition scans, indicating that air is also trapped within these features. However, in other cases, this assumption is not valid. For example, with thieno-PhOPh, a decrease in θ_w to 65.9° after 3 scans is observed because, as mentioned previously in the discussion, the nanopores on this surface are the largest in this study ($\varnothing \approx 500$ nm) and therefore, the assumption of trapped air within these features is no longer valid. In this case, the decrease in θ_w can be explained with the Wenzel equation because the larger porous structures enable complete penetration by water, a quality typical of Wenzel wetting.[33]

In order to better evaluate the influence of the water content on the formation of nanoporous membranes, the solvent CH₂Cl₂ + H₂O was simply diluted by CH₂Cl₂. The percentages tested were 35 and 65% of CH₂Cl₂ + H₂O versus CH₂Cl₂. The monomer selected was thieno-NaPh. First of all, we observe a huge influence of the water content (Figure 5). At a low water content [CH₂Cl₂ + H₂O (35%)], the formation of vertically aligned nanotubes is observed. The diameter of the nanotubes was roughly 200 nm and height 300 nm. However, the number of nanotubes was not very important. Here, when the water content increases, it was observed a huge increase of the number of nanotubes while their diameter and height remain unchanged [CH₂Cl₂ + H₂O (65%)]. Here, the formation of nanoporous membranes is obtained especially with 100% of CH₂Cl₂ + H₂O.

3. CONCLUSIONS

In this work, we demonstrate the ability to obtain nanotubular and nanoporous structures using a templateless electro-polymerization method in the organic solvent (CH₂Cl₂) and

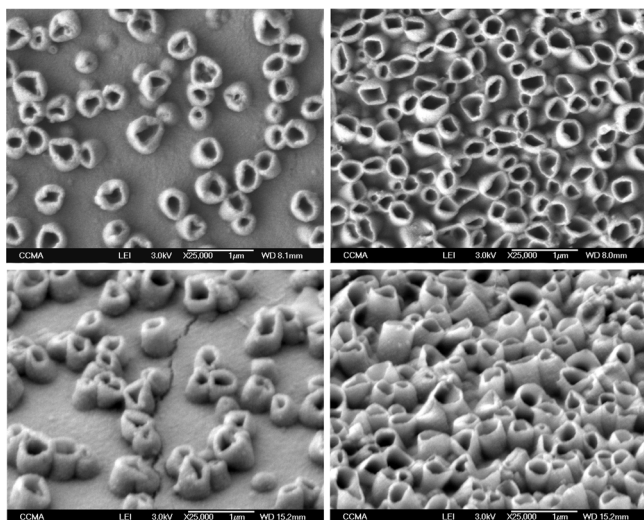**CH₂Cl₂ + H₂O (35%) Thieno-NaPh CH₂Cl₂ + H₂O (65%)**
3 scans

Figure 5. On the top, SEM images of polymer surfaces obtained from electrodeposition of thieno-NaPh in CH_2Cl_2 + H_2O (35%) and CH_2Cl_2 + H_2O (65%) via cyclic voltammetry after 3 scans. On the bottom, the same surfaces but with an inclination angle of 45°.

without the aid of a surfactant. Using thieno[3,4-b]thiophene monomers with rigid substituents, such perfluorinated chains or aromatic groups, nanoporous membranes were obtained when a significant fraction of water was included in the electrodeposition solvent (e.g., CH_2Cl_2 + H_2O). The inclusion of water in the solvent mixture drove this surface formation, as surfaces formed via electrodeposition in neat CH_2Cl_2 were relatively smooth. We also clearly demonstrated using different water contents that the formation of nanoporous membranes pass through the formation of vertically aligned nanotubes and that the increase in water content induced an increase in the number of nanotubes while their diameter and height remained unchanged. For the nanoporous surfaces, the pore size and the surface hydrophobicity were tunable by selection of the appropriate monomer. For example, an increase in hydrophobicity was observed with increasing pore size up to ≈300 nm, after which decreasing hydrophobicity was noted. Many applications could be envisaged for these surfaces in separation membranes, opto-electronic devices or sensors.

4. EXPERIMENTAL SECTION

4.1. Monomer Synthesis. Thieno[3,4-b]thiophene-2-carboxylic acid (thieno-COOH) was synthesized in three steps from 3,4-dibromothiophene (Scheme 2), as reported in the literature.[34−36] Then, 1.5 equiv of thieno-COOH was mixed with 1.5 equiv of N-(3-dimethylaminopropyl)-N'-ethylcarbodiimide hydrochloride and a catalytic amount of 4-(dimethylamino)pyridine in 20 mL of absolute acetonitrile.

Scheme 2. Synthetic Route for Monomers Studied
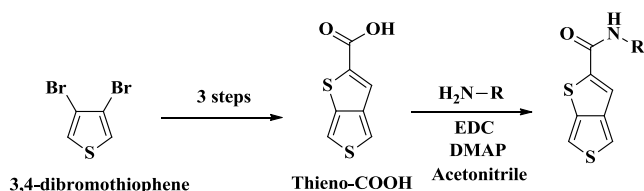
After stirring at ambient conditions for 30 min, 1 equiv of the corresponding amine was introduced to the mixture and left stirring. After 48 h, the crude product was purified via gel chromatography (eluent: cyclohexane/diethyl ether 50:50). The NMR details are given in the Supporting Information.

4.2. Electrochemical Depositions. Electrochemical depositions were performed using a potentiostat (Metrohm Autolab) equipped with a three-electrode system consisting of a gold plate (2 cm²) as the working electrode, a carbon-rod as the counter electrode, and a SCE as the reference electrode. The electrochemical cell was first filled with 10 mL of the solvent containing 0.1 M of tetrabutylammonium perchlorate (Bu_4NClO_4) as the electrolyte, as well as 0.01 M of the monomer of interest. Two different solvents were employed in order to better evaluate the influence of H_2O content: neat dichloromethane (CH_2Cl_2) and dichloromethane saturated with water (CH_2Cl_2 + H_2O). The latter was prepared by mixing CH_2Cl_2 with a high amount of deionized H_2O. To have precise desired H_2O fraction, any additional H_2O remaining after mixing was removed by extraction. It should be noticed that the solubility of water in dichloromethane is very low, around 0.17 g/100 mL, which means there is around 17 mg in the electrochemical cell we used (10 mL).

After determination of the oxidation potential (E^{ox}) for each synthesized monomer, templateless electrodepositions were performed under potentiodynamic conditions via cyclic voltammetry at a scan rate of 20 mV s⁻¹. The total number of scans was varied (1, 3, and 5) in order to characterize polymer growth. After electrodeposition, substrates were washed three times in dichloromethane to remove any unreacted monomer or nonadhered oligomers.

4.3. Surface Characterization. Surface morphology was investigated via scanning electron microscopy (SEM) using a JEOL 6700F microscope. Surface wettability was characterized by goniometry using a DSA30 goniometer (Bruker) and the "drop shape analysis system" software. Water droplets (2 μL) were deposited onto surfaces and the apparent contact angles (θ_w) were determined at the triple point. Each data point presented reflects a mean of five measurements (n = 5).

■ ASSOCIATED CONTENT

Ⓢ Supporting Information
The Supporting Information is available free of charge on the ACS Publications website at DOI: 10.1021/acsomega.9b00969.

Monomer characterization (PDF)

■ AUTHOR INFORMATION

Corresponding Author
*E-mail: thierry.darmanin@unice.fr.

ORCID Ⓘ
Frédéric Guittard: 0000-0001-9046-6725
Thierry Darmanin: 0000-0003-0150-7412

Notes
The authors declare no competing financial interest.

■ REFERENCES

(1) Cheng, Y.; Yang, H.; Yang, Y.; Huang, J.; Wu, K.; Chen, Z.; Wang, X.; Lin, C.; Lai, Y. Progress in TiO₂ Nanotube Coatings for Biomedical Applications: A Review. *J. Mater. Chem. B* **2018**, *6*, 1862−1886.

(2) Kwon, O. S.; Park, S. J.; Lee, J. S.; Park, E.; Kim, T.; Park, H.-W.; You, S. A.; Yoon, H.; Jang, J. Multidimensional Conducting Polymer Nanotubes for Ultrasensitive Chemical Nerve Agent Sensing. *Nano Lett.* **2012**, *12*, 2797−2802.

(3) Balasubramani, S. G.; Singh, D.; Swathi, R. S. Noble Gas Encapsulation into Carbon Nanotubes: Predictions from Analytical Model and DFT Studies. *J. Chem. Phys.* **2014**, *141*, 184304.

(4) Cheng, Z.; Gao, J.; Jiang, L. Tip Geometry Controls Adhesive States of Superhydrophobic Surfaces. *Langmuir* **2010**, *26*, 8233−8238.

(5) Ge, L.; Sethi, S.; Ci, L.; Ajayan, P. M.; Dhinojwala, A. Carbon Nanotube-Based Synthetic Gecko Tapes. *Proc. Natl. Acad. Sci. U.S.A.* **2007**, *104*, 10792−10795.

(6) Xu, M.; Du, F.; Ganguli, S.; Roy, A.; Dai, L. Carbon Nanotube Dry Adhesives with Temperature-Enhanced Adhesion over a Large Temperature Range. *Nat. Commun.* **2016**, *7*, 13450.

(7) Al-Azawi, A.; Latikka, M.; Jokinen, V.; Franssila, S.; Ras, R. H. A. Friction and Wetting Transitions of Magnetic Droplets on Micropillared Superhydrophobic Surfaces. *Small* **2017**, *13*, 1700860.

(8) Yu, S.; Guo, Z.; Liu, W. Biomimetic Transparent and Superhydrophobic Coatings: From Nature and Beyond Nature. *Chem. Commun.* **2015**, *51*, 1775−1794.

(9) Kowalski, D.; Schmuki, P. Polypyrrole Self-Organized Nanopore Arrays Formed by Controlled Electropolymerization in TiO₂ Nanotube Template. *Chem. Commun.* **2010**, *46*, 8585−8587.

(10) Lin, H.-A.; Luo, S.-C.; Zhu, B.; Chen, C.; Yamashita, Y.; Yu, H.-h. Molecular or Nanoscale Structures? The Deciding Factor of Surface Properties on Functionalized Poly(3,4-ethylenedioxythiophene) Nanorod Arrays. *Adv. Funct. Mater.* **2013**, *23*, 3212−3219.

(11) Pishkar, N.; Ghoranneviss, M.; Ghorannevis, Z.; Akbari, H. Study of the Highly Ordered TiO₂ Nanotubes Physical Properties Prepared with Two-Step Anodization. *Results Phys.* **2018**, *9*, 1246−1249.

(12) Paulose, M.; Prakasam, H. E.; Varghese, O. K.; Peng, L.; Popat, K. C.; Mor, G. K.; Desai, T. A.; Grimes, C. A. TiO₂ Nanotube Arrays of 1000 μm Length by Anodization of Titanium Foil: Phenol Red Diffusion. *J. Phys. Chem. C* **2007**, *111*, 14992−14997.

(13) Lee, W.; Park, S.-J. Porous Anodic Aluminum Oxide: Anodization and Templated Synthesis of Functional Nanostructures. *Chem. Rev.* **2014**, *114*, 7487−7556.

(14) Yuan, J.; Qu, L.; Zhang, D.; Shi, G. Linear Arrangements of Polypyrrole Microcontainers. *Chem. Commun.* **2004**, 994−995.

(15) Debiemme-Chouvy, C. One-Step Electrochemical Synthesis of a Very Thin Overoxidized Polypyrrole Film. *Electrochem. Solid-State Lett.* **2007**, *10*, No. E24.

(16) Fakhry, A.; Cachet, H.; Debiemme-Chouvy, C. Mechanism of Formation of Templateless Electrogenerated Polypyrrole Nanostructures. *Electrochim. Acta* **2015**, *179*, 297−303.

(17) Fakhry, A.; Pillier, F.; Debiemme-Chouvy, C. Templateless Electrogeneration of Polypyrrole Nanostructures: Impact of the Anionic Composition and pH of the Monomer Solution. *J. Mater. Chem. A* **2014**, *2*, 9859−9865.

(18) Debiemme-Chouvy, C. A Very Thin Overoxidized Polypyrrole Membrane as Coating for Fast Time Response and Selective H₂O₂ Amperometric Sensor. *Biosens. Bioelectron.* **2010**, *25*, 2454−2457.

(19) Debiemme-Chouvy, C. Template-Free One-Step Electrochemical Formation of Polypyrrole Nanowire Array. *Electrochem. Commun.* **2009**, *11*, 298−301.

(20) Qu, L.; Shi, G.; Yuan, J.; Han, G.; Chen, F. e. Preparation of Polypyrrole Microstructures by Direct Electrochemical Oxidation of Pyrrole in an Aqueous Solution of Camphorsulfonic Acid. *J. Electroanal. Chem.* **2004**, *561*, 149−156.

(21) Qu, L.; Shi, G.; Chen, F. e.; Zhang, J. Electrochemical Growth of Polypyrrole Microcontainers. *Macromolecules* **2003**, *36*, 1063−1067.

(22) Parakhonskiy, B.; Shchukin, D. Polypyrrole Microcontainers: Electrochemical Synthesis and Characterization. *Langmuir* **2015**, *31*, 9214−9218.

(23) Parakhonskiy, B.; Andreeva, D.; Möhwald, H.; Shchukin, D. G. Hollow Polypyrrole Containers with Regulated Uptake/Release Properties. *Langmuir* **2009**, *25*, 4780−4786.

(24) Kim, J. T.; Seol, S. K.; Je, J. H.; Hwu, Y.; Margaritondo, G. The Microcontainer Shape in Electropolymerization on Bubbles. *Appl. Phys. Lett.* **2009**, *94*, 034103.

(25) Debiemme-Chouvy, C.; Fakhry, A.; Pillier, F. Electrosynthesis of Polypyrrole Nano/Micro Structures using an Electrogenerated Oriented Polypyrrole Nanowire Array as Framework. *Electrochim. Acta* **2018**, *268*, 66−72.

(26) Darmanin, T.; Guittard, F. A One-Step Electrodeposition of Homogeneous and Vertically Aligned Nanotubes with Parahydrophobic Properties (High Water Adhesion). *J. Mater. Chem. A* **2016**, *4*, 3197−3203.

(27) Szczepanski, C. R.; M'Jid, I.; Darmanin, T.; Godeau, G.; Guittard, F. A Template-Free Approach to Nanotube-Decorated Polymer Surfaces using 3,4-phenylenedioxythiophene (PhEDOT) Monomers. *J. Mater. Chem. A* **2016**, *4*, 17308−17323.

(28) Ramos Chagas, G.; Darmanin, T.; Godeau, G.; Guittard, F. Nanocups and Hollow Microspheres Formed by a One-Step and Templateless Electropolymerization of Thieno[3,4-*b*]thiophene Derivatives as a Function of the Substituent. *Electrochim. Acta* **2018**, *269*, 462−478.

(29) Ramos Chagas, G.; Darmanin, T.; Guittard, F. One-Step and Templateless Electropolymerization Process using Thienothiophene Derivatives to Develop Arrays of Nanotubes and Tree-Like Structures with High Water Adhesion. *ACS Appl. Mater. Interfaces* **2016**, *8*, 22732−22743.

(30) Ramos Chagas, G.; Akbari, R.; Godeau, G.; Mohammadizadeh, M.; Guittard, F.; Darmanin, T. Electrodeposited Poly(thieno[3,2-*b*]thiophene) Films for the Templateless Formation of Porous Structures by Galvanostatic and Pulse Deposition. *ChemPlusChem* **2017**, *82*, 1351−1358.

(31) Bai, S.; Hu, Q.; Zeng, Q.; Wang, M.; Wang, L. Variations in Surface Morphologies, Properties, and Electrochemical Responses to Nitro-Analyte by Controlled Electropolymerization of Thiophene Derivatives. *ACS Appl. Mater. Interfaces* **2018**, *10*, 11319−11327.

(32) Cassie, A. B. D.; Baxter, S. Wettability of Porous Surfaces. *Trans. Faraday Soc.* **1944**, *40*, 546−551.

(33) Wenzel, R. N. Resistance of Solid Surfaces to Wetting by Water. *Ind. Eng. Chem.* **1936**, *28*, 988−994.

(34) Buemi, G. Molecular and Electronic Structures of Thieno[3,4-*b*]thiophene-2-carboxylic Acid and Acetic Thieno[3,4-*b*]thiophene-2-carboxylic Anhydride. An AM1, MNDO, and CNDO/S Study. *Bull. Chem. Soc. Jpn.* **1989**, *62*, 1262−1268.

(35) Wada, Y.; Asada, Y.; Ikai, T.; Maeda, K.; Kuwabara, T.; Takahashi, K.; Kanoh, S. Synthesis of Thieno[3,4-*b*]thiophene-Based Donor Molecules with Phenyl Ester Pendants for Organic Solar Cells: Control of Photovoltaic Properties via Single Substituent Replacement. *ChemistrySelect* **2016**, *1*, 703−709.

(36) Saji, V. S.; Zong, K.; Pyo, M. NIR-absorbing Poly(thieno[3,4-*b*]thiophene-2-carboxylic acid) as a Polymer Dye for Dye-sensitized Solar Cells. *J. Photochem. Photobiol., A* **2010**, *212*, 81−87.